J. Geophys. Eng. **9** (2012) 12–18 doi:10.1088/1742-2132/9/1/002

Separating P- and S-waves in an affine coordinate system

Jun Lu[1], **Yun Wang**[1,2,4] **and Chen Yao**[3]

[1] Key Laboratory of Marine Reservoir Evolution and Hydrocarbon Accumulation Mechanism, Ministry of Education, China University of Geosciences, Beijing 100083, People's Republic of China
[2] Institute of Geochemistry, Chinese Academy of Sciences, Guiyang 550002, People's Republic of China
[3] Institute of Multi-Component Seismic Technology, Beijing 100029, People's Republic of China

E-mail: lujun615@163.com and yunwang@mail.iggcas.ac.cn

Received 12 April 2011
Accepted for publication 18 October 2011
Published 12 December 2011
Online at stacks.iop.org/JGE/9/12

Abstract
This paper explores a method to separate P- and S-waves from multi-component seismic data utilizing wave vector rotation in an affine coordinate system. We use a vector composition method within a sliding time window to derive non-orthogonal P- and S-wave vector directions. Then all wave vectors within the sliding window are decomposed into the parallel and orthogonal parts in the direction of the P- or S-wave vector, in order to recover true amplitude P- and S-waves. The parallel part is reserved as the true amplitude signal, while the orthogonal part is eliminated as the residual noise. We examine the behaviour of the method when applied to synthetic data with different signal-to-noise ratios. The method is also demonstrated to be effective on field seismic records.

Keywords: multi-component seismic, mode leakage, affine coordinate system, wave separation

1. Introduction

In land multi-component seismic surveys, both P- and S-waves are expected to yield more information about the internal characteristics of a reservoir than P-waves have done (Stewart *et al* 2002, 2003, Zhao and Wang 2004). It is often assumed in multi-component seismics that the vertical component principally records pure-mode P-wave reflections and the horizontal component mainly contains mode-converted S-wave energy (Al-anboori *et al* 2005). This assumption is appropriate when a low-velocity near-surface layer exists and can make ray paths almost vertical to the surface. However, many field records show that the assumption fails with increasing offset or existence of high-velocity near-surface layers. The phenomenon known as 'mode leakage' can be measured, that is the potential cross-contamination of P-wave energy on the horizontal component, and S-wave energy on the vertical component (Guevara *et al* 1999). Suppressing 'mode leakage', namely P- and S-wave separation, is beneficial to shear-wave splitting analysis and imaging. In this paper, we propose a simple and direct wave vector rotation transformation method in the affine coordinate system to separate and recover P- and S-waves.

Methods have been proposed to separate P- and S-waves using the different characteristics in frequency, apparent velocity, polarization and so on, which can be categorized into two groups. One group is the scalar-processing methods, such as the f-k (Dankbaar 1985) or τ-p method (Stoffa *et al* 1981, Donati and Stewart 1996). With these methods, one can remove the contaminating wave energies in each component based on domain transformation. But the P- and S-wave amplitudes left in the vertical and horizontal components, respectively, are only the projections, not true amplitudes, which is not enough for the subsequent shear-wave splitting analysis and imaging. The second group is the vector-processing methods, such as direct mapping or the polarization filtering method. With these, one can separate different wave modes and meanwhile recover their amplitudes based on polarization characteristics. The polarization characteristics, elliptic or directional, are usually provided by the standard covariance method (SCM). Flinn (1965) originally proposed the SCM to compute the polarization ellipse within sliding time windows for

[4] Author to whom any correspondence should be addressed.

distinguishing different particle motions. Jurkevics (1988) applied the SCM to the polarization analysis of three-component seismic array data. Benhama *et al* (1988), Perelberg *et al* (1994) and Morozov *et al* (1996) also researched the SCM to separate P- and S-waves. Bataille *et al* (1991), Cho *et al* (1992), Franco *et al* (2001), Diallo *et al* (2006) and Lu *et al* (2010) proposed some improvements. Yan and Sava (2009, 2011) applied the method to separate wavefields using the polarization vectors, by solving the Christoffel equations. The method is applicable to anisotropic media if the corresponding Christoffel equation is used and the anisotropic parameters of the media are known. However, the orthogonal polarizations of P- and S-waves are assumed in the above vector-processing methods, which cannot separate and recover the true amplitudes of P- and S-waves thoroughly in a Cartesian coordinate system. This is because, in theory, P- and S-waves always polarize non-orthogonally at any reflection moment.

It is known that not assuming orthogonality is more robust theoretically to the wave separation problem, which was demonstrated by Li and Crampin (1993) in the separation of split S-waves. In this paper, we present a new method to separate P- and S-waves in non-orthogonal space. We establish an affine coordinate tensor matrix at receiver position to rotate wave vectors from the vertical and horizontal components to the true P- and S-wave vector directions. We also propose a composition method suitable for seismic data with a low signal-to-noise ratio to obtain wave vector directions. Finally, we demonstrate the method using real seismic field records.

2. P- and S-wave separation in an affine coordinate system

2.1. Basic assumptions

We assume the media is two-dimensional (2D) isotropic, VTI or azimuthal anisotropic and the *X*-component of the geophone is orientated to the source–receiver azimuth. When the media is 2D isotropic or VTI, 'mode leakage' can only be recorded by the *Z*- and *X*-components, and the *Y*-component records noise only (Yan and Sava 2009). If the 2D media is azimuthal anisotropic, the S-waves can split into the fast (S1) and slow (S2) modes (Crampin 1981). In that situation, both S1- and S2-waves will form an interference wavelet, which can be decomposed into an SV-wave polarizing in the *Z*–*X* plane and an SH-wave polarizing in the *Y*-direction (Alford 1986, Tsvankin *et al* 2010). 'Mode leakage' should be suppressed in the *Z*–*X* plane, because only P- and SV-waves can be observed on both the *Z*- and *X*-components, and P-waves cannot be recorded by the *Y*-component on the assumption that the media is 2D (Thomsen 1988).

2.2. Rotation transformation equation

We use **P** and **S** to denote P- and S-wave vectors in the *Z*–*X* plane. In the ground receiver position, we establish an *X*–*O*–*Z* coordinate system with two axes in the directions of the *Z*- and *X*-components, and assume the reflected waves are propagating from the underground towards the first quadrant (figure 1). The P- and S-wave vectors are

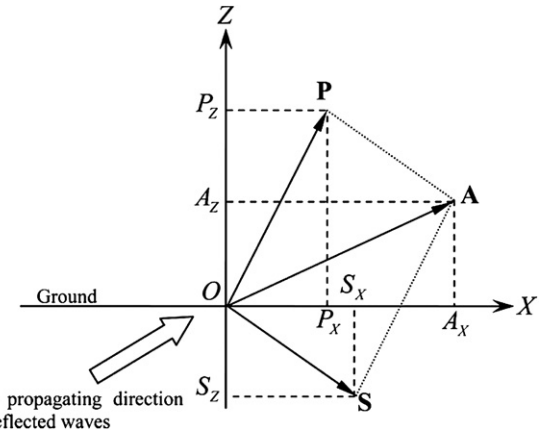

Figure 1. Schematic diagram of the P- and S-wave vectors in the *X*–*O*–*Z* coordinate system.

$$\begin{cases} \mathbf{P} = P_X \mathbf{e}_X + P_Z \mathbf{e}_Z \\ \mathbf{S} = S_X \mathbf{e}_X + S_Z \mathbf{e}_Z \end{cases}, \tag{1}$$

where $\mathbf{e}_X$ and $\mathbf{e}_Z$ are the base vectors in the *X*- and *Z*-directions, respectively. As wave vectors **P** and **S** are non-orthogonal, traditional wave separation methods in the Cartesian coordinate system cannot completely separate the P- and S-waves. In this paper, we perform the wave separation in an affine coordinate system, in which the two axes are in the directions of the wave vectors **P** and **S**. The base vectors of the P- and S-axes are denoted by $\mathbf{e}_P$ and $\mathbf{e}_S$, respectively.

Let us make a composite vector $\mathbf{A} = \mathbf{S} + \mathbf{P}$, which can be derived as

$$\mathbf{A} = (P_X + S_X)\mathbf{e}_X + (P_Z + S_Z)\mathbf{e}_Z, \tag{2}$$

where projections in the *X*- and *Z*-directions of the Cartesian coordinate system are **X** and **Z**, and $\mathbf{A} = \mathbf{X} + \mathbf{Z} = A_X\ \mathbf{e}_X + A_Z\ \mathbf{e}_Z$. Then we can use an affine coordinate tensor matrix to rewrite equation (2) as

$$\begin{bmatrix} \mathbf{Z} \\ \mathbf{X} \end{bmatrix} = \begin{bmatrix} \cos(\mathbf{e}_P, \mathbf{e}_Z) & \cos(\mathbf{e}_S, \mathbf{e}_Z) \\ \cos(\mathbf{e}_P, \mathbf{e}_X) & \cos(\mathbf{e}_S, \mathbf{e}_X) \end{bmatrix} \begin{bmatrix} \mathbf{P} \\ \mathbf{S} \end{bmatrix}, \tag{3}$$

where the tensor matrix transforms the P- and S-waves from the affine coordinate system *P*–*O*–*S* to the Cartesian coordinate system *X*–*O*–*Z*.

To separate the P- and S-wave vectors, a rotation transformation equation can be derived from equation (3) as

$$\begin{bmatrix} \mathbf{P} \\ \mathbf{S} \end{bmatrix} = \begin{bmatrix} \cos(\mathbf{e}_P, \mathbf{e}_Z) & \cos(\mathbf{e}_S, \mathbf{e}_Z) \\ \cos(\mathbf{e}_P, \mathbf{e}_X) & \cos(\mathbf{e}_S, \mathbf{e}_X) \end{bmatrix}^{-1} \begin{bmatrix} \mathbf{Z} \\ \mathbf{X} \end{bmatrix}. \tag{4}$$

Therefore, from equation (4), it can be seen that the directions of the base wave vectors should be determined firstly for separating the P- and S-wave vectors.

2.3. Determination of the base wave vector

We use a vector composition method to obtain the base wave vectors. Let us begin with an example where the angle between **P** and the positive *Z*-axis is 30°, and that between **S** and the positive *Z*-axis is 110°. Figure 2(*a*) plots P- and

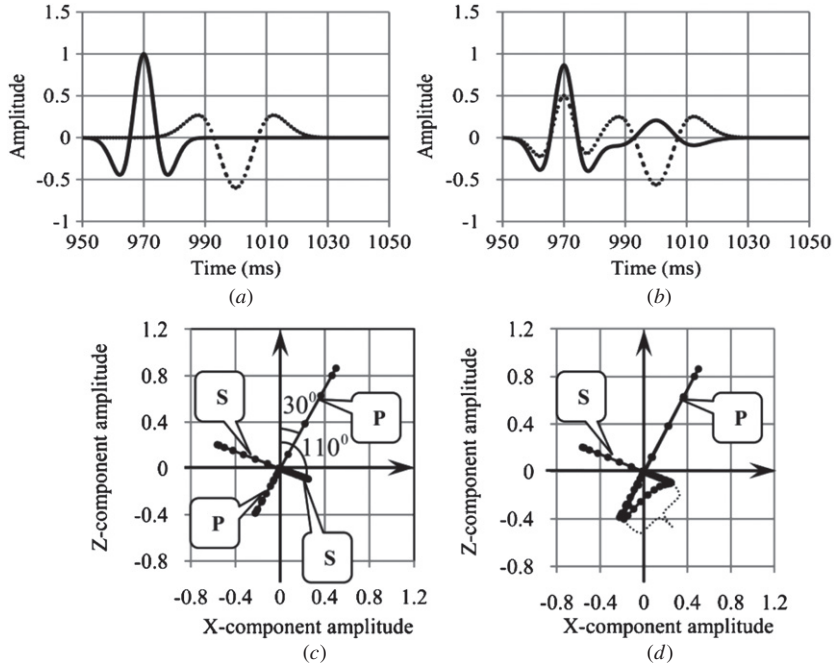

Figure 2. (*a*) Synthetic P-wave (solid line) and S-wave (dashed line). (*b*) Synthetic *Z*-component (solid line) and *X*-component (dashed line). (*c*) Polarization graph of pure P- and S-waves in the *X*–*O*–*Z* coordinate system. (*d*) Polarization graph of *Z*- and *X*-component waves when 'mode leakage' occurs.

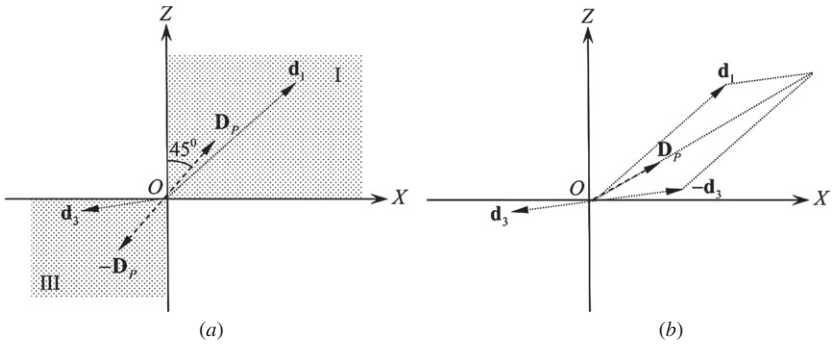

Figure 3. (*a*) Initial $\mathbf{D}_P$, and vectors $\mathbf{d}_1$ and $\mathbf{d}_3$, derived separately in the first iteration from the composition of all the wave vectors in the shadow zones I and III. (*b*) Updated $\mathbf{D}_P$ from the composition of $\mathbf{d}_1$ and $\mathbf{d}_3$ after the first iteration.

S-waves recorded in the *P*–*O*–*S* coordinate system, which are transformed into the *X*–*O*–*Z* coordinate system using equation (3), as shown in figure 2(*b*).

Figure 2(*c*) is the polarization graph of the **P** and **S** vectors (pure P- and S-waves, in a window of 950–1050 ms) in the *X*–*O*–*Z* system. Analysing this polarization graph, we can see that they all polarize linearly, and that the wave vector **P** locates in the first and third quadrants, and the wave vector **S** locates in the second and fourth quadrants. However, in figure 2(*d*), the polarization graph of the **Z** and **X**-vectors (figure 2(*b*)) shows 'mode leakage'. Partial P- and S-wave vectors can hardly be differentiated in the third and fourth quadrants (marked by a dashed bracket).

We determine the base wave vectors iteratively (figure 3). During the first iteration, set two wave vector composition zones I and III (shadow zones in figure 3(*a*)) to cover the first and third quadrants, into which the *P*-wave vectors should be located, then the initial angle-bisector unit vector in zone I is set to be $\mathbf{D}_P$, and that in zone III is $-\mathbf{D}_P$, where

$$\mathbf{D}_P = \tfrac{1}{\sqrt{2}}\mathbf{e}_X + \tfrac{1}{\sqrt{2}}\mathbf{e}_Z. \tag{5}$$

Compose the entire wave vectors in zone I to get vector $\mathbf{d}_1$, and those in zone III to get vector $\mathbf{d}_3$ (figure 3(*a*)). Reverse vector $\mathbf{d}_3$ to get $-\mathbf{d}_3$, and compose it with $\mathbf{d}_1$ to derive an updated $\mathbf{D}_P$ (figure 3(*b*)) as

$$\mathbf{D}_P = \begin{cases} \dfrac{\mathbf{d}_1 - \mathbf{d}_3}{|\mathbf{d}_1 - \mathbf{d}_3|}, & \mathbf{d}_1 \neq \mathbf{d}_3 \\ 0, & \mathbf{d}_1 = \mathbf{d}_3 = 0 \\ \dfrac{\mathbf{d}_1}{|\mathbf{d}_1|}, & (\mathbf{d}_1 = \mathbf{d}_3) \neq 0. \end{cases} \tag{6}$$

Use the new $\mathbf{D}_P$ and $-\mathbf{D}_P$, respectively, to update the corresponding wave vector composition zones I and III for the second iteration. After several iterations, the variation of

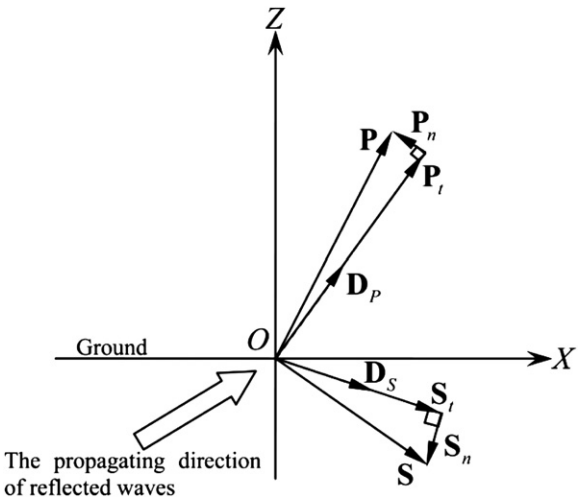

Figure 4. Schematic diagram of the P- and S-wave vector decomposition.

$\mathbf{D}_P$ will be subtle, and the processing can be stopped, then a quite precise P-wave unit vector $\mathbf{D}_P$ will be obtained.

For the S-wave, set the initial angle-bisector unit vector $\mathbf{D}_S = 1/\sqrt{2}\mathbf{e}_X - 1/\sqrt{2}\mathbf{e}_Z$, and $-\mathbf{D}_S$ in zones II and IV, corresponding to the second and fourth quadrants. Performing the corresponding wave vector composition in the same way as $\mathbf{D}_P$, we can obtain the S-wave unit vector $\mathbf{D}_S$.

The ultimate $\mathbf{D}_P$ and $\mathbf{D}_S$ are considered as the base wave vector $\mathbf{e}_P$ and $\mathbf{e}_S$ and their directions are used in equation (4) for separating P- and S-wave vectors. Respectively, the parallel part $\mathbf{P}_t$ or $\mathbf{S}_t$ of $\mathbf{P}$ or $\mathbf{S}$ (figure 4) can be written as

$$\begin{cases} \mathbf{P}_t = \mathbf{D}_P \cdot \mathbf{P} \\ \mathbf{S}_t = \mathbf{D}_S \cdot \mathbf{S} \end{cases} \tag{7}$$

which is reserved as the true amplitude signal. And the orthogonal part $\mathbf{P}_n$ or $\mathbf{S}_n$ as

$$\begin{cases} \mathbf{P}_n = \mathbf{P} - \mathbf{P}_t \\ \mathbf{S}_n = \mathbf{S} - \mathbf{S}_t \end{cases} \tag{8}$$

is eliminated as the residual noise.

This wave separation process is performed sample-by-sample within a sliding time window which is centred at the sample. At any reflection moment, the S-wave has a longer period than the P-wave because of the different subsurface absorptions. In the S-wave period, there is more than one period of P-wave, so the P-wave frequency band (f_l, f_u) can be used to decide the length of sliding window (Kallweit *et al* 1982). To guarantee stability, we set the length of the sliding time window used for P- and S-wave separation in the area $(1/f_u, 1/f_l)$.

3. Application examples

3.1. Numerical example

First we show the test on synthetic data with noise. Figures 5(*a*) and (*b*) are the *Z*- and *X*-components of the synthetic waves shown in figure 2(*b*), but with additional random noise of 10% and 50%, respectively. For the case with 10% noise, we can distinguish the wave vectors from the polarization graph with little difficulty, as shown in figure 5(*c*). However, for the case with 50% noise, we can hardly distinguish them (figure 5(*d*)).

We use the vector composition method described above to obtain the directions of $\mathbf{e}_P$ and $\mathbf{e}_S$. Figures 6(*a*) and (*b*) show the iterative updating of the angle between $\mathbf{P}$ and the positive *Z*-axis, and that between $\mathbf{S}$ and the positive *Z*-axis.

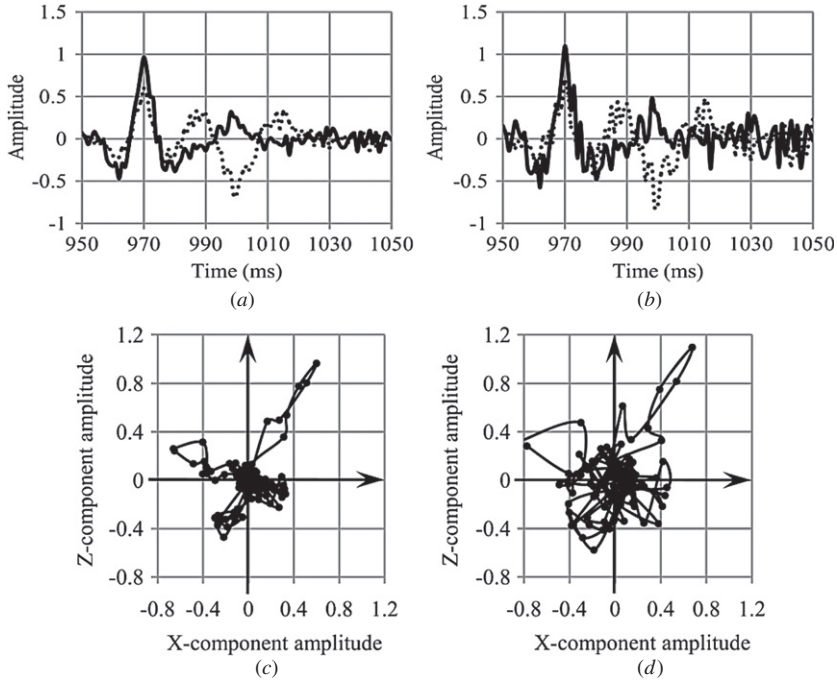

Figure 5. Synthetic *Z*- (solid line) and *X*-component (dashed line) waves with (*a*) 10%, and (*b*) 50% random noise. Polarization graph of *Z*- and *X*-component waves with (*c*) 10%, and (*d*) 50% random noise.

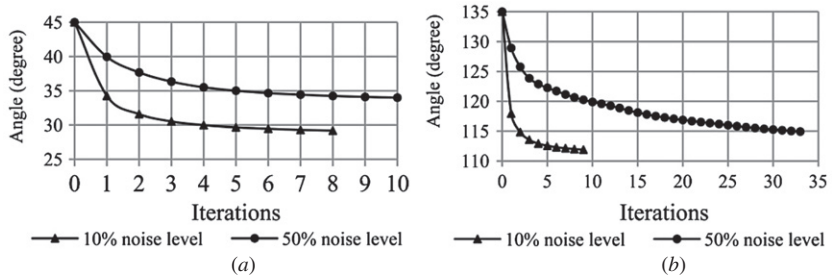

Figure 6. Update of the angle between (*a*) **P** and the positive *Z*-axis and (*b*) **S** and the positive *Z*-axis during the iteration.

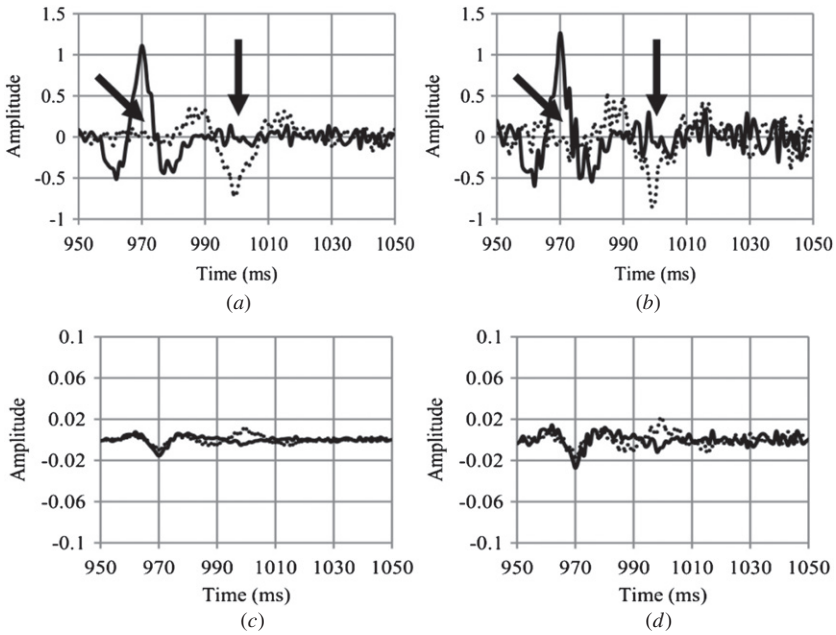

Figure 7. Wave separation with (*a*) 10% random noise, and (*b*) a 50% random noise level (solid line: P-wave, dashed line: S-wave). With noise suppressed from *Z*- (solid line) and *X*-component waves (dashed line) at a (*c*) 10% random noise level and (*d*) a 50% random noise level.

When the noise level is low, we can derive very precise wave vector directions. Even when the noise level is high, a stable and close result can be derived with many more iterations.

Figures 7(*a*) and (*b*) show the wavefield separation results for the cases with 10% and 50% noise, respectively. They demonstrate that when the wavefield separation method is effective, even the data are polluted with noise. In particular in the areas marked by arrows, we can see that the wavefields are separated out and the majority of real amplitude is recovered. Figures 7(*c*) and (*d*) are the residuals, which do show some 'mode leakage'. However, the amplitude scales of these two figures are reduced to nearly 10% of those in figures 7(*a*) and (*b*), and the residual is in fact quite small.

3.2. Real data example

Figure 8 shows the field applications of P- and S-wave separation in the same amplitude scale. Figures 8(*a*) and (*b*) are field *Z*- and *X*-component shot records with low signal-to-noise ratios, where 'mode leakage' is marked by the black arrow. To keep the polarization characteristics, only a 5–80 Hz band-pass filtering is applied to suppress the noise. Figures 8(*c*) and (*d*) show recovered P- and S-waves (in particular in the elliptic frame marking places), from which we can see that P-wave first arrivals leaked to the *X*-component are suppressed to a large extent in the hollow arrow marking places. Figures 8(*e*) and (*f*) show, respectively, the 'mode leakage' of the S-wave recorded by the *Z*-component and that of the P-wave recorded by the *X*-component. It can be seen that the *X*-component is more contaminated than the *Z*-component because the emergent angles of reflected P-waves are larger than those of converted S-waves. Many similarities can be found between figures 8(*d*) and (*e*) or figures 8(*c*) and (*f*) on the time characteristics of the events, which could indicate that the separating method for P- and S-waves proposed in the paper is effective.

4. Discussion

During the procedure of real data processing, we found that, if the energy of a sharp pulse or Rayleigh waves is too strong, the vector composition method would be unlikely to have a good result even after repeated iterations. We have shown that some pre-processing procedures are needed for the raw field data to suppress such noise. But it should be guaranteed that such

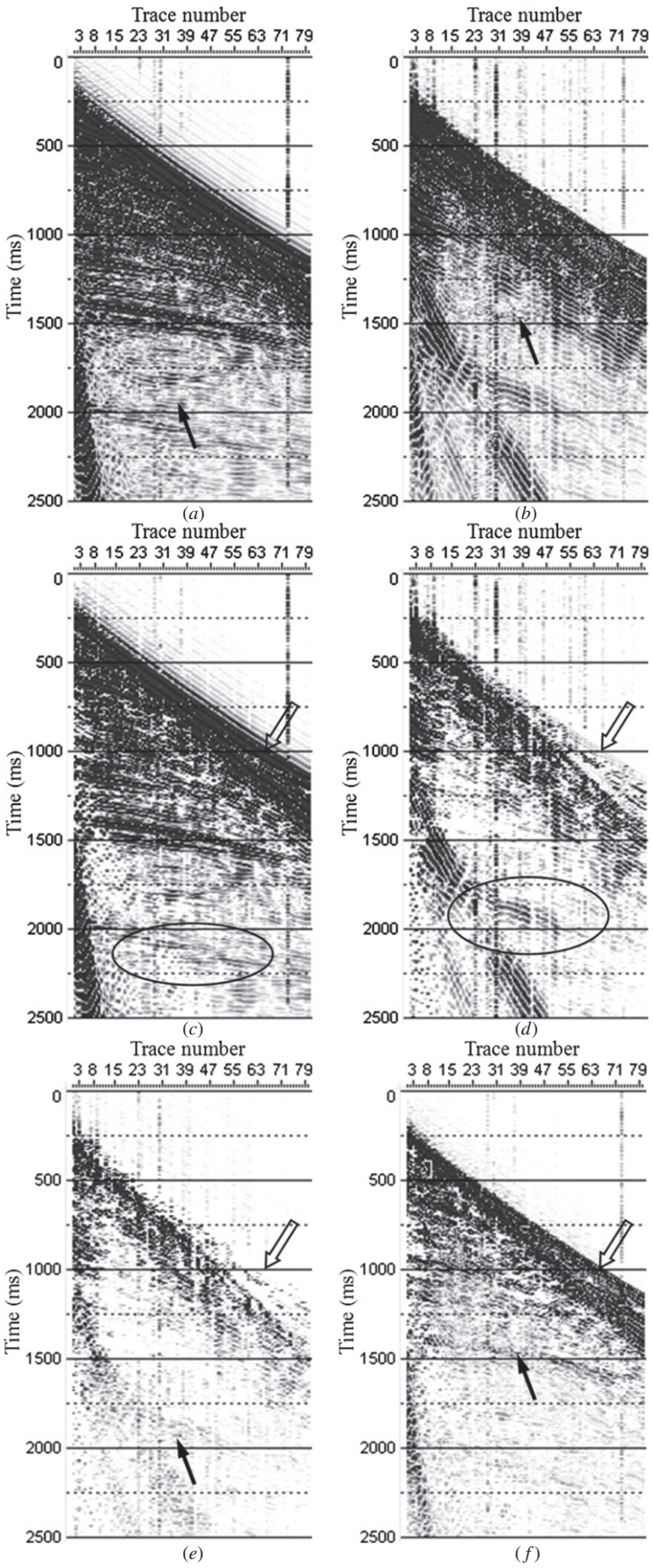

Figure 8. (*a*) Field *Z*-component waves. (*b*) Field *X*-component waves. (*c*) P-waves separated out. (*d*) S-waves separated out. (*e*) The 'mode leakage' of S-waves received in the *Z*-component. (*f*) The 'mode leakage' of P-waves received in the *X*-component.

procedures would not change the polarization characteristics of the P- and S-waves recorded by the *Z*- and *X*-components.

For three-dimensional three-component (3D3C) seismic exploration, sometimes wave separation in the *Z–X* plane is not enough. 3D3C seismic wave processing flow should start with a horizontal rotation, which is used to rotate one of the horizontal components to the radial (source–receiver) direction (*R*-component) and the other to the transverse direction (*T*-component). If the subsurface is flat-layered, only P- and SV-waves polarize in the *Z–R* plane and they can be separated using the same method proposed in this paper. But in a wide variety of circumstances, ubiquitous spatial or azimuthal variations of rock properties often make P- and split S-modes from different depths interfere and project onto all three components. In this situation, 'mode leakage' will be more complicated. Thus, efforts should be directed to develop a more powerful method to separate P- and split S-modes using all three components.

5. Conclusions

P- and S-wave separation is important for the subsequent shear-wave splitting analysis and imaging, because 'mode leakage' often occurs when the offset is increased or the high-velocity near-surface layer exists. On the assumption that the media is 2D isotropic, VTI or azimuthal anisotropic, 'mode leakage' only occurs in the *Z–X* plane. Even if the media is 3D anisotropic, P- and S-waves are only needed to be separated in the *Z–R* plane if the subsurface is flat-layered. But this assumption is not suitable when spatial or azimuthal variations of rock properties exist.

Because P- and S-waves always polarize non-orthogonally at any reflection moment, they cannot be separated in the Cartesian coordinate system. In this paper, we have shown how to separate P- and S-waves in the 2D model, by a rotation transformation from the Cartesian coordinate system *X–O–Z* to an affine coordinate system *P–O–S*. During the procedure, the directions of the base vectors, which can be derived by a vector composition approach, are important to establish the affine coordinate tensor matrix. Testing of the synthetic data shows that the approach can achieve stable and close wave vector directions even with low signal-to-noise ratios, but more iterations are needed.

In the real data application, the polarization characteristics of P- and S-waves should be guaranteed in the pre-processing procedures, before separating wavefields using our method. The application results for both synthetic and real data also demonstrate that our method can separate P- and S-waves robustly without the assumption of orthogonal polarization through the affine coordinate transformation.

Acknowledgments

This research is supported by the Fundamental Research Funds for the Central Universities (no 2011YYL043), NSFC (no 4110484) and National Special Fund (no 2011ZX05035-001-006HZ, 2011ZX05035-003-006HZ, 2011ZX05008-006-022).

References

Al-anboori A, Baan M and Kendall J M 2005 Approximate separation of pure-mode and converted waves in 3-C reflection seismic by τ-p transform *Geophysics* **70** pp 81–6

Alford R 1986 Shear data in the presence of azimuthal anisotropy *56th Annu. Int. Meeting, SEG, Expanded Abstracts* pp 476–79

Bataille K and Chiu J M 1991 Polarization analysis of high-frequency three-component seismic data *Bull. Seismol. Soc. Am.* **81** 622–42

Benhama A, Cliet C and Dubesset M 1988 Study and applications of spatial directional filtering in three-component recordings *Geophys. Prospect.* **36** 591–613

Cho W H and Spencer T W 1992 Estimation of polarization and slowness in mixed wavefields *Geophysics* **57** 805–14

Crampin S 1981 A review of wave motion in anisotropic and cracked elastic-media *Wave Motion* **3** 343–91

Dankbaar J W 1985 Separation of P- and S-waves *Geophys. Prospect.* **33** 970–86

Diallo M S, Kulesh M, Holschneider M, Kurennaya K and Scherbaum F 2006 Instantaneous polarization attributes based on an adaptive approximate covariance method *Geophysics* **71** 99–104

Donati M S and Stewart R R 1996 P- and S-wave separation at a liquid–solid interface *J. Seismic Explor.* **5** 113–27

Flinn E A 1965 Signal analysis using rectilinearity and direction of particle motion *Proc. IEEE* **53** 1874–6

Franco R and Musacchio G 2001 Polarization filter with singular value decomposition *Geophysics* **66** 932–8

Guevara S E and Cary P W 1999 Wavefield separation in the presence of statics: application to synthetic and real data *CREWES Research Report* 11 vol 32 pp 1–20

Jurkevics A 1988 Polarization analysis of three-component array data *Bull. Seismol. Soc. Am.* **78** 1725–43

Kallweit R S and Wool L C 1982 The limits of resolution of zero-phase wavelet *Geophysics* **47** 1035–46

Li X Y and Crampin S 1993 Linear-transform techniques for processing shear-wave anisotropy in four-component seismic data *Geophysics* **58** 240–56

Lu J, Wang Y and Yang C Y 2010 Instantaneous polarization filtering focused on suppression of surface waves *Appl. Geophys.* **7** 88–97

Morozov L B and Smithson S B 1996 Instantaneous polarization attributes and directional filtering *Geophysics* **61** 872–81

Perelberg A I and Hornbostel S C 1994 Applications of seismic polarization analysis *Geophysics* **59** 119–30

Stewart R R, Gaiser J E, Brown R J and Lawton D C 2002 Converted-wave seismic exploration: methods *Geophysics* **67** 1348–63

Stewart R R, Gaiser J E, Brown R J and Lawton D C 2003 Converted-wave seismic exploration: applications *Geophysics* **68** 40–57

Stoffa P L, Buhl P, Diebold J and Wenzel F 1981 Direct mapping of seismic data to the domain of intercept time and ray parameter—A plane-wave decomposition *Geophysics* **46** 255–67

Thomsen L 1988 Reflection seismology over azimuthally anisotropic media *Geophysics* **53** 304–13

Tsvankin I, Gaiser J, Grechka V, Van M and Thomsen L 2010 Seismic anisotropy in exploration and reservoir characterization: an overview *Geophysics* **75** 75A15–29

Yan J and Sava P 2009 Elastic wave-mode separation for VTI media *Geophysics* **74** WB19–32

Yan J and Sava P 2011 Improving the efficiency of elastic wave-mode separation for heterogeneous tilted transverse isotropic media *Geophysics* **76** T65–78

Zhao S and Wang Y 2004 Relative amplitude preserved PP and PSV wave seismic sections *J. Geophys. Eng.* **1** 259–62